NON-PERTURBING MEASUREMENTS OF INTERPARTICLE FORCES AND RHEOLOGICAL PROPERTIES IN COLLOIDAL WIGNER CRYSTALS

Report of MSc thesis research, conducted at the Laboratory of Physical Chemistry and Colloid Sciences, Wageningen UR

Author Marieke Gerth

Supervisors Ruben Higler & Joris Sprakel

Examiner Jasper van der Gucht

MSc. Thesis Physical Chemistry and Colloid Science

Period June 11th 2014 – November 3rd 2014

Location Laboratory of Physical Chemistry and Colloid Science, Wageningen University

Student Marieke Gerth
marieke.gerth@wur.nl

Supervisors Ruben Higler
ruben.higler@wur.nl

Joris Sprakel
joris.sprakel@wur.nl

Examiner Jasper van der Gucht
jasper.vandergucht@wur.nl

SUMMARY

In this research, we pioneer in developing a method, based on optical microscopy, to probe the mechanical properties of supersoft materials without making assumptions or perturbing the material. Mechanical properties, such as shear modulus, are a commonly used parameter to characterise materials. By fitting our experimental data to a screened Coulomb potential, a Yukawa potential, we extract parameters characterising the interactions in our system, needed for further calculations on interparticle forces. The derivative of the pair potential equation is equal to the force between two particles at centre-to-centre distance *r*. We calculate the shear relaxation based on particle-particle interactions and the mean square displacement to support the validity of our method to probe the shear relaxation of a supersoft solid.

TABLE OF CONTENTS

LIST OF ABBREVIATIONS

ACF	autocorrelation function
AoT	dioctyl sodium sulfosuccinate
EtOH	ethanol
fps	frames per second
HMDS	hexamethyldisilazane
MSD	mean square displacement
PMMA	poly(methyl methacrylate)
RDF	radial distribution function
TEOS	tetraethyl orthosilicate
tetralin	1,2,3,4-tetrahydronaphtalene

1. INTRODUCTION

Numerous methods are known to probe the mechanical properties of solids. Dynamics can be assessed through scattering experiments, phase transitions can be assessed through calorimetry, and mechanical properties like responses to shear and stress can be assessed through standard rheology. The properties of interest in rheological experiments are the material's moduli, which reflect the mechanical properties. The magnitude of the moduli scales with the energy of interaction between two particles, multiplied by the density.[1] This means that, for solids, moduli are in the order of GPa. For colloidal systems, such as those studied here, according to the scaling theory, the mechanical moduli roughly fall in the μPa-mPa range, which is too low to be assessed by classical rheology.

Several other methods have been developed to measure the moduli of supersoft solids. Micro-rheology[2] can be used to directly probe the mechanical properties of the medium surrounding the probe particle, in this case a colloidal system. Micro-rheology cannot be used in this research, as the theory of this method assumes a homogeneous medium[3] or a hard-sphere system,[4] which is not the case in our experiments. The dispersion relation, the study of the dispersion of waves within a sample, is another method used to assess the mechanical properties of supersoft solids.[5] This theory is based on the assumption that the system is undamped, which is usually not the case, because particles are dispersed in a medium.

The research described here is aimed at developing a novel method to assess the mechanical properties of supersoft solids without making any assumptions. To achieve this, we first have to characterise the interactions between the Wigner particles studied here. Wigner particles are like-charged and thus repel each other, following a screened Coulomb potential[6, 7] (Yukawa potential, Equation 1). It is vital that the Wigner particles are suspended in an apolar medium,[8] so that dipoles of the medium do not interfere with the repellent charges of the particles. To extract the relevant Yukawa parameters for our system without making assumptions, we use an inversion based on the Ornstein-Zernike equation to obtain the pair potential from our experimental data.[8]

$$\frac{U(r)}{k_B T} = \frac{\varepsilon\sigma}{r} \cdot exp[-\kappa\sigma\left(\frac{r}{\sigma} - 1\right)] \quad (1)$$

We use Wigner particles in this research because they form crystalline-like ordered structures at low densities, but Brownian fluctuations prevent true long-range ordering. These features cause Wigner crystals to fall in between classical solids and liquids, and make researching these materials challenging but interesting.

An important part of the research reported here is based on characterising the forces between particles. Measuring these forces is a laborious experiment. The forces may be directly measured by optical tweezer experiments,[9] or extrapolated from a dilution series to correct for multi-particle interactions.[10] In this research we use a facile method to calculate the force between two neighbouring particles as a function of their separation distance. Using this method, only particle positions are needed to calculate all interparticle forces in a sample. After we elucidate the pair potential for our system, we calculate the interparticle forces using the derivative of the equation which describes the pair potential (Equation 2).

$$\frac{|F(r)|}{k_BT} = \frac{1}{k_BT} \cdot \left|\frac{dU(r)}{dr}\right| = \left| -\frac{\varepsilon\sigma}{r^2} \cdot (\kappa r + 1) \cdot \exp[\kappa(\sigma - r)] \right| \quad (2)$$

In a static crystal, forces are balanced and equal because of the regular structure in a crystal. Here, we investigate colloidal crystals, and liquids, in which particles are free to move around their lattice points. This causes variations in interparticle forces, and possibly sample spanning networks of forces larger than average. Snoeijer and co-workers showed the existence of these force networks in granular materials in stable, confined, static packings and under shear.[11] This research aims at demonstrating the existence of force networks in the Wigner crystals studied here. By doing so, we intend to show that the differences between granular and crystalline materials are smaller than commonly accepted.

We use the possibility to calculate interparticle forces to assess the mechanical properties of the Wigner crystals and liquids studied here. The Brownian fluctuations enable us to probe the time dependent mechanical response to shear without active perturbation of the system. By assessing the movement of particles, and the response of surrounding particles, we can probe the systems response to (internal) shear and assess the relaxation of the system. The shear relaxation, relaxation time and moduli that may be obtained by this analysis are the mechanical properties of the system we intend to elucidate in this research. By analysing the mean square displacement for the different phases, we can supplement the analysis of the shear stress relaxation.

2. EXPERIMENTAL

2.1 MATERIALS

AoT (98%), HMDS (≥99%) and TEOS (99.999%) were purchased from Sigma-Aldrich. 4μm silica particles were purchased from Cospheric innovations. Ammonia solution (25%) was purchased from Emsure. Ethanol (absolute) was purchased from Merck. Decane was purchased from TCI. All chemicals were used as received. 3μm fluorescent PMMA particles were prepared by this lab using a previously reported protocol.[12]

2.2 INSTRUMENTATION

FLUORESCENCE AND PHASE CONTRAST MICROSCOPE

Fluorescence and phase contrast microscopy is carried out on a Zeiss Axiovert 200 equipped with a 20x objective and a Thorlabs DCU224 camera.

BRIGHTFIELD MICROSCOPE

Brightfield microscopy is carried out on a Nikon eclipse Ti-U equipped with a Nikon plan Apo λ 20x0.75 WD1.0 objective and a Fastec Imaging HiSpec1 2G Mono camera.

2.3 SAMPLE PREPARATION

We prepare samples by introducing a suspension of PMMA particles in 10mM AoT in decane in glass sample chambers, and hermetically sealing them with optical adhesive. Before filling, sample chambers are flushed with acetone and propanol, dried under nitrogen flow and then dried for 1hr at 60°C. The chambers are then plasma cleaned, filled with HMDS, and dried at 60°C. The crystals are confined to 2D by gravitation. The PMMA particles are charged by enveloping them in AoT micelles.

2.4 DATA ANALYSIS

Several Matlab codes are used in the data analysis, the basics of each code are described in this section.

PARTICLE LOCATING

The freely available Kilfoil particle locating algorithms,[13] are used to analyse image sequences. The code searches for a local maximum in intensity, and then fits a Gaussian distribution to the peak in intensity to locate the centre of the object at a sub-pixel resolution.

RADIAL DISTRIBUTION FUNCTION

The script we use to calculate the 2D radial distribution function determines the number of particles in a shell of thickness dr at a distance r, up to a maximum r_{max} of each reference particle. This number is then normalized for the surface of the shell so that $g(r)$ converges to a value of 1 for large r.

PAIR POTENTIAL

The method we use in this research to calculate the pair potential from the RDF is based on earlier research.[8] Because we do not work at infinite dilution, we have to take indirect interactions between particles in account, which complicates calculation of the pair potential. First, we calculate the total correlation function $h(r) = g(r) - 1$. Then, we use an optimized

method[14] to Fourier transform h(r) and write the direct interactions in terms of the total and indirect interactions (c(r)) using the Ornstein-Zernike equation in Fourier space. Through the hypernetted chain function, we relate h(r), and thus g(r), to the pair potential. The solved equation is inverse-Fourier transformed to real space to obtain the direct interactions. Then, we calculate U(r) via the following relation: $U(r) = h(r) - c(r) - \log(g(r))$.

FORCE DISTRIBUTION

The script we use to calculate the force distribution in a sample takes the Yukawa potential parameters ε, σ and κ as input, and with the particle coordinates for each frame, obtained from the Kilfoil tracking algorithm, calculates the forces between each pair of nearest neighbours as identified by a Delaunay triangulation. A probability distribution is calculated by logarithmic binning of all obtained forces and normalizing for the number of particle pairs found.

FORCE MAPS

Using the same method to calculate forces between nearest neighbours as in the force distribution code, and the particle coordinates in each frame as obtained from the Kilfoil tracking algorithm, we can plot force maps, in which forces between nearest neighbours are plotted for each frame. The code plots the forces between neighbours as thick, dark lines, of decreasing thickness and darkness with decreasing force. For clarity, the script also plots the scaled outline of the particles.

ORIENTATIONAL BOND ORDER PARAMETER

The script to calculate the orientational bond order parameter, Ψ_6, uses the particle coordinates in each frame to calculate the $\Psi_6$value for each particle using Equation 3:[15]

$$\psi_6 = \frac{1}{n_c}\sum_{j=1}^{n_c} e^{i6\theta(ij)} \quad (3)$$

which is explained in detail in the next chapter. Again, nearest neighbours are identified using a Delaunay triangulation.

DE-DRIFTING AND BEAD ID

The standard Kilfoil algorithm for de-drifting determines the collective motion of all particles in one specific direction over the whole data-set, assumes a constant speed of the particles, and uses this information to redefine the position of each particle at each time point so that only Brownian motion remains. We use a modified method to de-drift the image sequences by determining the collective motion of all particles in one specific direction per frame. The script for de-drifting also connects particle positions between two subsequent frames, and appoints an ID to every bead, so that each bead's trajectory can be tracked in time.

SHEAR RELAXATION MODULUS

With the particle positions for each frame, the frame rate and a method to calculate the forces between particles, we calculate the shear relaxation modulus, $G_{2D}(t)$, by correlating two dimensional shear stresses between particle pairs in time (Equation 4-6).

$$G_{2D}(t) = \frac{A}{2} \cdot \left|\langle s_{xy}(t) \cdot s_{xy}(t-t')\rangle\right| + \left|\langle s_{yx}(t) \cdot s_{yx}(t-t')\rangle\right| \quad (4)$$

In Equation 4, A is the area of the field of view, k_b the Boltzmann constant, T the temperature in K, and s_{xy} the two dimensional shear stress defined as:

$$s_{xy} = \frac{1}{A}\sum_{i<j} F_{ij,y}\Delta x_{ij} \quad (5)$$

with Δx_{ij} the difference in x-coordinates between particles *i* and *j*, and $F_{ij,y}$ the force in the y-direction between particles *i* and *j* in k_bT. S_{yx} is defined as:

$$s_{yx} = \frac{1}{A}\sum_{i<j} F_{ij,x}\Delta y_{ij} \quad (6)$$

With Δy_{ij} the difference in y-coordinates between particles *i* and *j*, and $F_{ij,x}$ the force in the x-direction between particles *i* and *j* in k_bT.

The compression, $K_{2D}(t)$, is calculated via similar equations:

$$K_{2D}(t) = \frac{A}{2} \cdot |\langle s_{xx}(t) \cdot s_{xx}(t-t')\rangle| + |\langle s_{yy}(t) \cdot s_{yy}(t-t')\rangle| \quad (7)$$

In which we take the force acting along the same axis as the one we use to calculate the distance between particles.

MEAN SQUARE DISPLACEMENTS

This script uses the output file of the de-drifting algorithm because the particles each have an appointed ID number. The squared displacements are calculated for each particle, between every possible pair of frames, after which the average displacement (squared) is divided by the number of data-points for that specific time-step to obtain the MSD in time.

3. RESULTS AND DISCUSSION

In this research, we pioneer in developing a method to probe the mechanical properties of supersoft materials without making assumptions or perturbing the material. Mechanical properties, such as the shear modulus, are a commonly used parameter to characterise materials. We calculate shear relaxation based on particle-particle interactions (Equation 4-6). In order to calculate the interactions, we need a way to measure the force between particles. The existing methods, as described briefly in the introduction, require extensive experimental work; we develop a facile method based on optical microscopy. We use the radial distribution function, which is a probability distribution of finding a particle at a certain centre-to-centre distance *r* (Section 3.1) to calculate the pair potential, the potential energy of two interacting particles at centre-to-centre distance *r* (Section 3.2). By fitting our experimental data to a screened Coulomb potential, a Yukawa potential, we extract parameters characterising the interactions in our system, needed for further calculations on interparticle forces. The derivative of the pair potential equation is equal to the force between two particles at centre-to-centre distance *r* (Section 3.3). With this new method to assess the interparticle forces in our system, we investigate the homogeneity of our samples by calculating force distributions (Section 3.3) and by assessing the crystallinity of the samples through visualisation of forces in force maps (Section 3.4). We use the orientational bond order parameter, Ψ_6, as a measure for the crystallinity of our samples (Section 3.4). Next, we calculate the 2D shear relaxation of samples in the liquid and crystalline phase, based on particle-particle interactions (Section 3.5). We calculate mean square displacements of the same two samples to support the validity of our method to probe the shear relaxation of a supersoft solid (Section 3.6).

3.1 RADIAL DISTRIBUTION FUNCTION

The first step in this research is to calculate the radial distribution function. The RDF, g(*r*), is a visualisation for the level of crystallinity of a, in this case 2D, colloidal system. The RDF is a probability distribution of finding a particle in a shell of thickness *dr* at distance *r* from a reference particle, and is used to analyse the level of order in the system. If the particles form a perfect static crystal lattice, the RDF will feature sharp peaks at distinct centre-to-centre distance *r*. Because we analyse a soft crystal in which the particles can fluctuate around their lattice points, the peaks in g(*r*) will broaden in comparison with a static crystal. If the system is diluted to a liquid, we expect only local ordering to remain and the RDF to converge to 1 for large *r*. In the RDFs shown here, we scaled the x-axis with the *r*-value of the first peak.

LIQUID PHASE

The RDF of a sample in the liquid phase (Figure 1a) shows evidence of local ordering, as indicated by the large peak, but no long range ordering. The first peak is quite broad, because the particle density is low enough in the liquid phase for the particles not to be 'confined' by surrounding particles. At a certain distance, the ordering is lost and the RDF converges to 1.

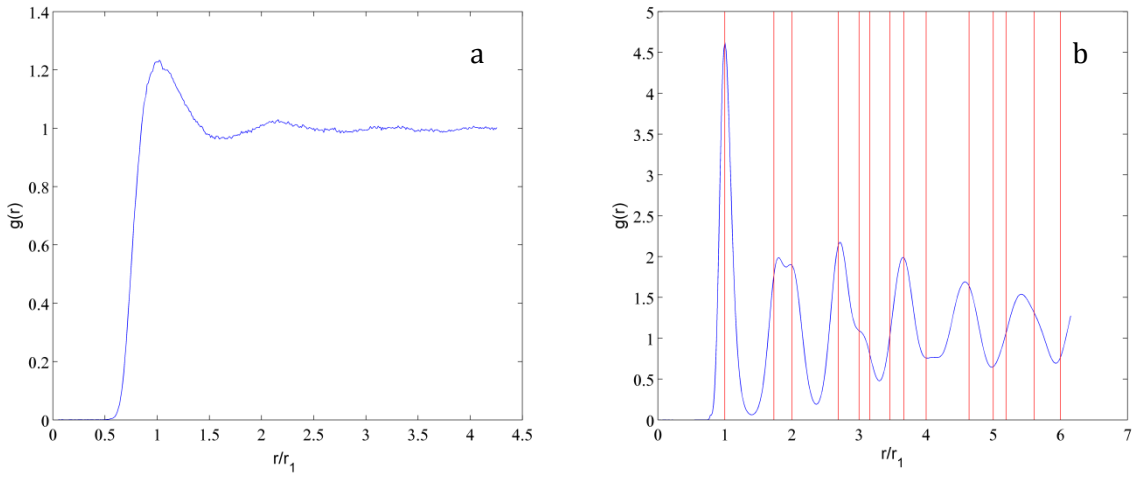

Figure 1|RDF of a sample in the liquid phase (a) with a density of $4.4 \cdot 10^{-3}$ particles per μm². The image sequence is recorded at 15 fps. The first peak corresponds to an interparticle distance of 10.5μm. RDF of a sample in the crystalline phase (b) with a density of $1.8 \cdot 10^{-2}$ particles per μm². The red vertical lines mark where we expect peaks for a hexagonal lattice. The image sequence is recorded at 0.5 fps. The first peak corresponds to an interparticle distance of 7.2μm.

CRYSTALLINE PHASE

The RDF of a crystalline sample (Figure 1b) shows presence of long range ordering, as indicated by the on-going peaks in the RDF at large distance from the reference particle. Due to the plasticity of these crystals, the peaks in the RDF of a crystalline sample will, at sufficient *r*, converge to 1, as in the liquid samples.

When comparing the peaks, especially the first, to the peak in the RDF of a liquid (Figure 1a), it is clear that the first peak is much sharper in the RDF of the crystalline sample, indicating that particles are 'confined' by their neighbours. For a perfect static hexagonal lattice, the first peaks in the RDF would be very sharp. As the particles in these crystals are not fixed in a perfect crystal lattice, but fluctuate around their lattice points, the peaks in the RDF of the Wigner crystal are broader, and prevent the RDF from reaching 0 in between peaks indicating absence of true long-ranged order.

Another feature that differs between the RDF of a liquid (Figure 1a) and a crystal (Figure 1b) is that the first peak in the RDF of the crystal is shifted to a lower absolute *r* value in comparison to the first peak in the RDF of the liquid, from 10.5μm in the liquid to 7.2μm in the crystal. This is explained by the higher density of particles in the crystal, causing the particles to be closer to each other.

The red vertical lines in Figure 1b mark where we expect peaks in a perfect hexagonal lattice. The peaks in our RDF agree well with the predicted values for the peaks, thereby proving we have a hexagonal lattice.

3.2 PAIR POTENTIAL

We use the RDF as calculated in Section 3.1 to calculate the pair potential. We use fluorescence microscopy and phase contrast microscopy data to measure the pair potential for the PMMA Wigner particles, and brightfield microscopy to measure the pair potential for the silica Wigner particles. The parameters we extract from fitting the pair potential are used to calculate interparticle forces in Sections 3.3-3.5.

The pair potential describes the interaction between two particles at infinite dilution. The particles in this system are like-charged, we thus expect purely repulsive interactions. Several methods are reported to measure the pair potential.

The optical tweezers may be used to measure the interactions between two particles, as described in literature.[9] Two particles are trapped using laser beams, and released when no other particles are near. By analysing the displacements in time of these particles, one can extract the pair potential.

The extrapolation method[10] is based on calculating the potential of mean force, W(r), from the radial distribution function via Equation 8. The potential of mean force, W(r), is only valid at finite dilution, whereas the pair potential, U(r), implies infinite dilution. By extrapolating the potential of mean force for various volume fractions to infinite dilution, one can estimate U(r).

$$\frac{W(r)}{k_B T} = -\ln[g(r)] \tag{8}$$

The more facile approach we use here requires analysis of only one sample. From the radial distribution function, g(r), we calculate the pair potential U(r) (Equation 1), provided the system is sufficiently diluted. We use a Yukawa potential of the form

$$\frac{U(r)}{k_B T} = \frac{\varepsilon\sigma}{r} \cdot exp[-\kappa\sigma\left(\frac{r}{\sigma} - 1\right)] \tag{1}$$

to fit the experimentally obtained pair potential to extract the parameters ε (repulsion at contact in k_BT), σ (particle radius in μm) and κ (Debye length in μm^{-1}). The Yukawa potential is only valid for solely repulsive interaction between particles, and thus is positive over the entire range, and decreases with increasing r.

FLUORESCENCE MICROSCOPY

The pair potential for PMMA particles obtained though fluorescence microscopy, Figure 2, features a slight negative dip, indicating that the sample may be too concentrated as will be discussed in more detail in this section. However, as the data fits the Yukawa potential quite well, we choose to use the extracted parameters (Table 1) from this experiment in the next steps of the data analysis of the PMMA particles in decane. We use experimentally obtained data for r larger than 7μm to fit the Yukawa potential (Equation 1) to.

Table 1|Values of parameters extracted from experimental data, obtained through fluorescence microscopy, using a Yukawa potential.

Parameter (units)	Value
ε (k_BT)	196
κ (μm^{-1})	0.844
σ (μm)	3.00

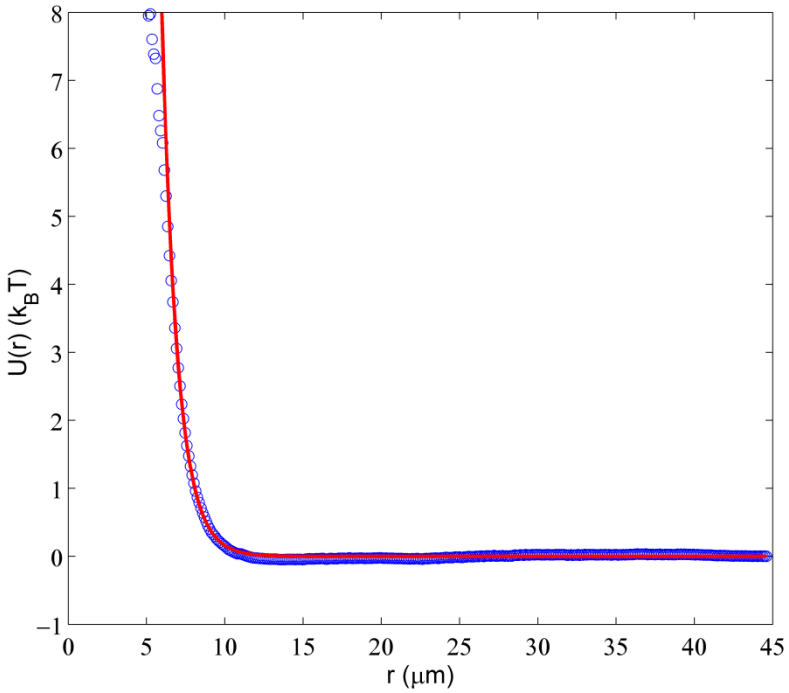

Figure 2|Experimentally obtained pair potential of a sample in the liquid phase with a density of $4.4 \cdot 10^{-3}$ particles per μm² (blue circles) and Yukawa potential modelled with obtained fitting parameters (red line). The image sequence is recorded at 15 fps.

BRIGHTFIELD MICROSCOPY

When the same method is used to extract Yukawa parameters for a sample of silica particles in tetralin from data obtained through brightfield microscopy, we were forced to use a modified Yukawa potential ($U_m(r)$, Equation 9); we added an emperial power law to the Yukawa potential enable fitting to the experimental data (Figure A1).The modified Yukawa potential allowed for attractive interactions between the particles, and was of the form

$$\frac{U_m(r)}{k_B T} = \frac{\varepsilon_r \sigma}{r} \cdot \exp\left[-\kappa\sigma\left(\frac{r}{\sigma} - 1\right)\right] - \varepsilon_a \left(\frac{r}{\sigma}\right)^{-\alpha} \tag{9}$$

In which ε_r is repulsion at contact (in k_BT), ε_a is attraction at contact (in k_BT), σ is the particle diameter (in μm), κ is the Debye length (in μm^{-1}), α is the powerlaw exponent, and *r* the centre-to-centre distance between particles. It must be noted that obtained parameters cannot be compared to those obtained in fluorescence or phase contrast mode. The extracted parameters from the modified Yukawa potential (Table 2) are used in further analysis of this particle-solvent system.

Table 2|Values of parameters extracted from experimental data using modified Yukawa model

Parameter (units)	Value
ε_r (k_BT)	116.57
κ (μm^{-1})	1.16
σ (μm)	3.98
ε_a (k_BT)	7.45
α	3.61

When our image sequences recorded though brightfield microscopy are used to calculate U(r), the pair potential drops below zero, which would indicate attraction. The cause of this attractive part in the pair potential is under debate in literature. Whereas some literature states that the attraction is real, and caused by interaction between charged particles and like-charged surfaces,[6, 16] the attractive dip is also reported to be an optical artefact in brightfield microscopy,[17] caused by Airy disks.

We speculated it is neither; these explanations only hold true for attractions between nearest neighbours. The attraction caused by interaction between particles and like-charged surfaces is only possible if particles are very close to one another and would therefore exist at lower r than we observe here. Likewise, Airy disks only overlap if the particles are very close. The attraction in our system spans all r from two particle radii and above. We speculate that the sample from which we obtained the pair potential though brightfield imaging was not sufficiently diluted, introducing errors in the calculation of the pair potential from the RDF.

PHASE CONTRAST MICROSCOPY

The pair potential of a PMMA particle system in the liquid phase, recorded through phase contrast microscopy did not exhibit a negative pair potential, but features a bump for large r (Figure A2), and thus attraction for large r. We hypothesise the bump is caused by diluting too far; the sample analysed through fluorescence microscopy has a number density of $4.4 \cdot 10^{-3}$ particles per μm^2, whereas the sample used in the phase contrast measurements has a number density of $2.0 \cdot 10^{-3}$ particles per μm^2. The absence of a negative dip supports our speculations of the previous samples being too dense. The absence of the negative dip, and presence of a positive bump for large r has a significant influence on the Yukawa parameters (Table 3). As mentioned earlier, we use the parameters obtained from fluorescence microscopy experiments for further analysis of the PMMA decane system.

Table 3|Parameters extracted from fit of Yukawa potential to calculated pair potential obtained through phase contrast microscopy.

Parameter (unit)	Value
ε (k_BT)	317
κ (μm^{-1})	0.687
σ (μm)	3.00

As the parameters extracted from the phase contrast microscopy experiments are quite different from those obtained though fluorescence microscopy experiments, the actual values used here may not be accurate, but observed trends in further data-analysis are still valid.

3.3 FORCE DISTRIBUTION

The parameters extracted by fitting the Yukawa potential to our experimentally obtained pair potential (Section 3.2) are used in this section to calculate the interparticle forces without perturbation of the system. We calculate a probability distribution of the forces in a liquid and crystalline sample, and use these to illustrate the difference in homogeneity between these states.

The repellent forces between the particles originate from the charge on each particle. If we assume every particle to have the same charge, both in sign and magnitude, the forces between

two particles vary only with their separation distance, following Coulombs laws. The derivative of the pair potential (Equation 1) yields |F(r)| (Equation 2), with which we can calculate the forces between two particles if we know their mutual distance.

$$\frac{U(r)}{k_B T} = \frac{\varepsilon\sigma}{r} \cdot \exp\left[-\kappa\sigma\left(\frac{r}{\sigma} - 1\right)\right] \tag{1}$$

$$\frac{|F(r)|}{k_B T} = \frac{1}{k_B T} \cdot \left|\frac{dU(r)}{dr}\right| = \left| -\frac{\varepsilon\sigma}{r^2} \cdot (\kappa r + 1) \cdot \exp[\kappa(\sigma - r)] \right| \tag{2}$$

To visualise how |F| evolves with r and to get an estimate of the size of the interparticle forces in this system, we plot |F(r)| (Equation 2) for relevant r using the parameters obtained in the previous section (Table 1). As the diameter of the particles used in this research is 3µm, this is the smallest centre-to-centre distance we could achieve during experiments. The force should be infinite for centre-to-centre distances than 3µm, as this would indicate interpenetration of particles. From Figure 3 we see that the forces associated with the smallest centre-to-centre distances possible in these samples are extremely small, ranging several piconewtons. Nearest neighbours separated by more than four times the particle diameter exert forces on each other in the femtonewton range. The exponential increase in forces between particles calls for very accurate particle tracking, as minute errors in interparticle distances have a major effect on the, faulty, force measured.

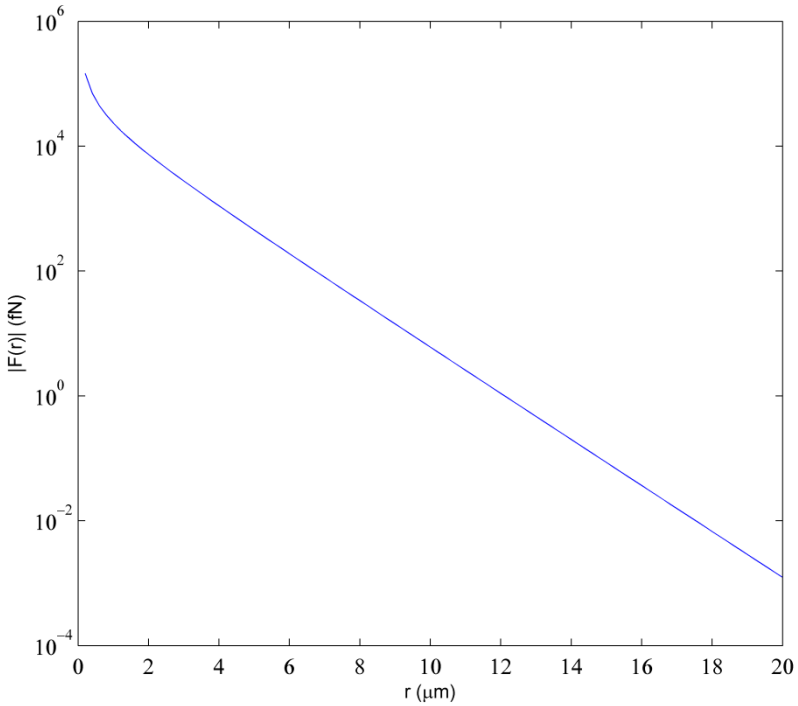

Figure 3|Evolution of |F| with increasing *r*.

By calculating all forces between nearest neighbours, we can construct a probability distribution of forces in the sample. We expect peaks in the force distribution, which become broader with decreasing density of the sample. The sharpness of the peak is indicative for the level of ordering of the system. Sharp peaks indicate homogeneous samples, in this case crystals, and broad peaks indicate low levels of ordering.

LIQUID PHASE

A sample in the liquid phase has a low density and, as a result, large interparticle distances when compared to the particle diameter. As the particles are free to move, the range of interparticle distances is expected to be quite large, resulting in a broad distribution of small forces between nearest neighbours. Due to the expected large range of forces present in this sample, we use logarithmic binning of forces to enable proper sampling of the small forces.

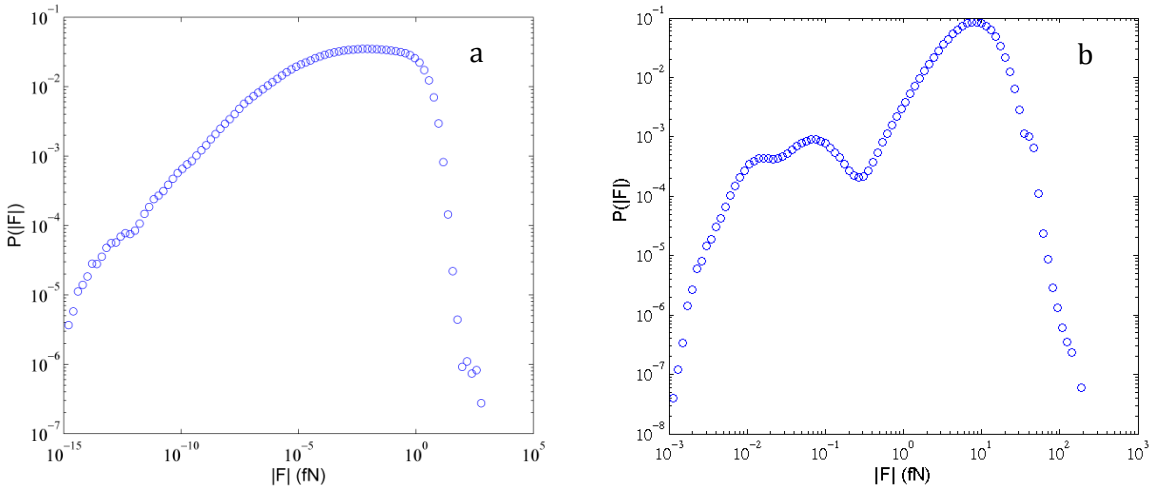

Figure 4|a) Distribution of forces in a sample in the liquid phase with a density of $4.4 \cdot 10^{-3}$ particles per µm². b) Distribution of forces in a sample in the crystalline phase with a density of $1.8 \cdot 10^{-2}$ particles per µm²

From the force distribution of a sample in the liquid phase (Figure 4a), it is clear that the particles are not 'confined' by their neighbours; the peak in the distribution is broad, spanning roughly 20 orders of magnitude. Due to the low density in the liquid sample, the particles are free to move, small forces are more abundant than the large forces, causing the tail of small forces. The average force in this sample is 0.26fN.

CRYSTALLINE PHASE

For a crystal in which particles occupy their hexagonal lattice points at all times, the force distribution is a delta-function. For an almost static crystal, we would expect a very sharp Gaussian peak, because the forces increase exponential with centre-to-centre distance, and we bin logarithmically. If the distribution of forces includes multiple orders of magnitude, as is the case in this research, we expect a deviation from the Gaussian shaped peak, because the exponential function and logarithm do not use the same number as a base.

For the PMMA crystal, however, we do not find a single peak (Figure 4b), but we rather find a second and third peak at smaller forces than average and a shoulder at larger than average forces. For a crystal of silica particles in tetralin we do find a sharp Gaussian peak (Figure A3). The Gaussian peak is present in the silica crystals because the silica system forms denser and more ordered crystals.

In a PMMA crystal, which is much denser than the liquid analysed in the previous section, the interparticle distances are smaller, so that the forces between particles are larger (Figure 4b). The average force for this sample is 8.22fN, approximately 30 times as high as in the liquid sample.

We hypothesise the extra peaks in the force distribution for the crystalline phase are caused by errors in particle locating. The interparticle distances indicated by the forces at the extra peaks roughly agree with the second and third peak in the RDF, indicating that the nearest neighbours we use to calculate forces are two lattice spaces removed from one another. Considering the plasticity of these crystals, and the size of this data set, in combination with the relatively high probability supports this hypothesis, as opposed to the existence of deletions in this crystal.

3.4 FORCE MAPS AND ORIENTATIONAL BOND ORDER PARAMETER

To visualise the difference in homogeneity between the liquid and crystalline samples (Section 3.3), we construct force maps. Using the equation for $|F(r)|$ (Equation 2) we can calculate the forces between each pair of particles in a frame. By plotting the forces between neighbouring particles through connecting them with lines that become increasingly dark and bold with increasing force, we construct force maps. In these force maps the homogeneity or heterogeneity of the force distribution in a snapshot of the sample can be visually analysed.

Heterogeneity in interparticle forces are caused by heterogeneities in distances between nearest neighbours. With variations in interparticle distances, the bond angle between nearest neighbours changes. To numerically analyse the (in-)homogeneity, or level of crystallinity, of a sample, we calculate the 2D orientational bond order parameter, ψ_6, defined as:[15]

$$\psi_6 = \frac{1}{n_c}\sum_{j=1}^{n_c} e^{i6\theta(ij)} \tag{3}$$

Where n_c is the number of nearest neighbours j around particle i with $\theta(r_{ij})$ the bond angle between particles i and j with an arbitrary yet fixed reference axis. In a perfect 2D hexagonal crystal lattice the orientational bond parameter equals 1, which decreases with decreasing sixfold symmetry.

In the rest of this section, it has to be taken into account that the colour coded ψ_6 can be directly compared between samples from the colours in the figures, but the forces were scaled per sample for clarity of the homogeneity or heterogeneity in individual phases.

LIQUID PHASE

The liquid phase has a low density, so we expect relatively large interparticle distances and a low average sixfold symmetry. Indeed, the average value of ψ_6 in this data set is 0.3810. As can be seen in the snapshot in Figure 5, most particles are separated by multiple particle diameters. Because of the low density, the particle are extremely mobile, we thus expect high variation in the average sixfold symmetry, as can be seen from the large variation in colour in Figure 5.

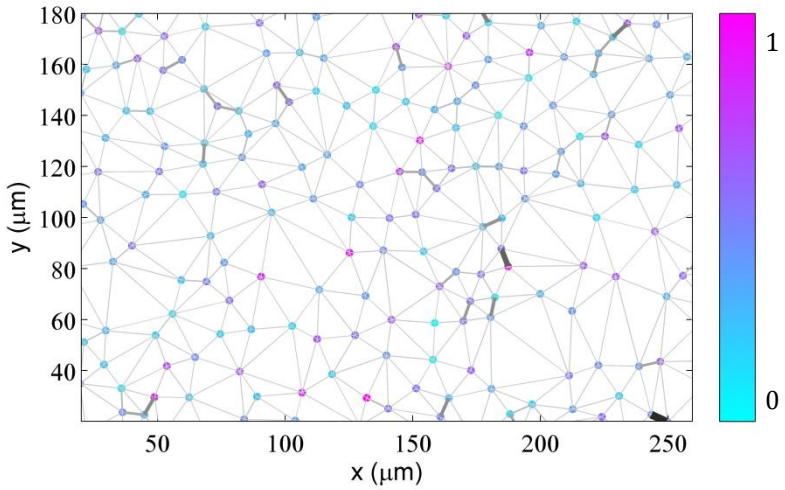

Figure 5|Force map constructed from a snapshot of a sample in the liquid phase with a density of $4.4 \cdot 10^{-3}$ particles per μm², the particles are coloured to their ψ_6 value.

CRYSTALLINE PHASE

A snapshot of the crystal (Figure 6), colour coded for ψ_6, still shows some inhomogeneity because of the fluctuations of the particles around their lattice points. The PMMA crystals are not very dense, so the particles in these crystals are not confined by their neighbours, allowing for relatively large displacements from the lattice points. The average ψ_6 value for the whole data set is 0.7524, which is quite low when compared with static crystals, but may be a reasonable value for a Wigner crystal.

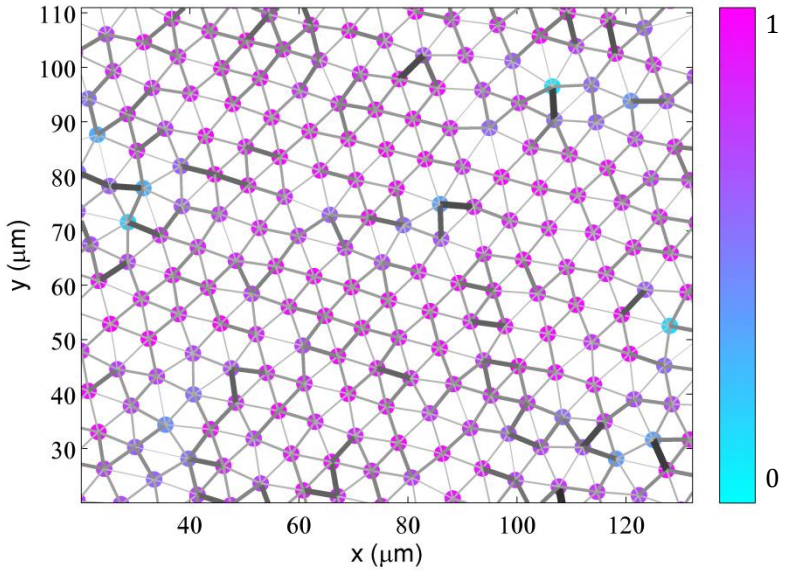

Figure 6|Force map constructed from a snapshot of a sample in the crystalline phase with a density of $1.8 \cdot 10^{-2}$ particles per μm², the particles are coloured to their ψ_6 value.

GRAIN BOUNDARY IN SiO_2 PARTICLE CRYSTAL

Because the PMMA particles form crystals with very few defects of only one specific type,[18] defects are studied in another particle-solvent system; SiO_2 particles (for particle modification, see Appendix A1) in 10mM AoT in tetralin sediment faster and have a lower mobility than the PMMA particles which enables the system to have large and long term defects. The Yukawa

parameters are different for this system, and we calculated the pair potential for this system (Section 3.2), to extract the relevant parameters (Table 2).

When comparing a ψ_6 colour coded snapshot of a silica particle crystal (Figure 7) with that of a PMMA particle crystal (Figure 6), it is clear that, despite the defects, the silica sample has a higher level of crystallinity, as evidenced by the difference in colour variety in the crystalline parts of the samples. Despite part of the crystal taking part in the grain boundary defect, the average ψ_6 for this sample is 0.9240, which indicates a high level of crystallinity. Part of the explanation of the higher level of crystallinity in the silica is the fact that the silica particles are much heavier than the PMMA particles, and thus exhibit less Brownian movement. Another explanation may be that the silica crystal has a number density of $4.0 \cdot 10^{-2}$ particles per μm^2, which is about twice as high as the number density in the PMMA crystal, causing the particles in the silica crystal to be more 'confined'.

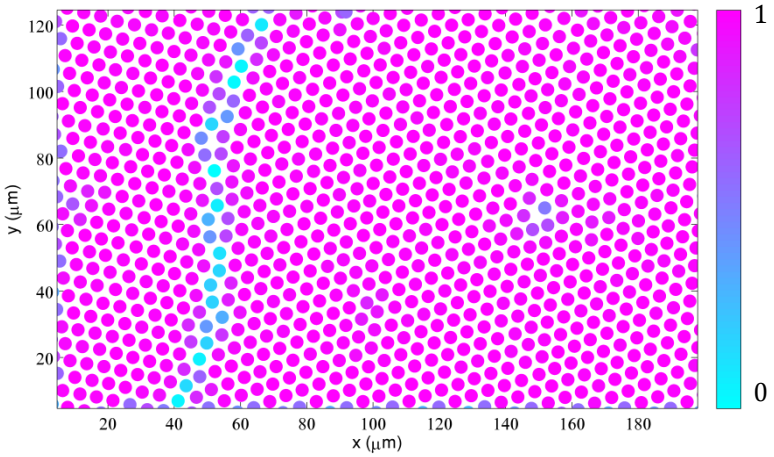

Figure 7|Snapshot of particle positions in a SiO_2 particles crystal with a grain boundary, colour coded for ψ_6 value.

In the force map of the same sample (Figure 8), it is clearly visible that the largest imbalance in forces is concentrated around the grain boundary. In bulk, the imbalance in forces, caused by the irregular ordering of particles, forms a weakness in the material. Due to the irregularities, applied forces and stress cannot be redistributed evenly over the entire sample, causing mechanical failure to initiate at these sites.

From the force map in Figure 8, we can also more clearly see that the grain boundary mainly consists of 5/7 defects. The defects in which 7 particles surround a central particle have, relatively, large forces between the particles in the 7-membered ring, and small forces between the particles in the ring and the central particle. In contrast, the defects in which only 5 particles surround a central particle, the forces between the particles in the ring are, relatively, small, and the forces between particles in the ring and the central particle are large.

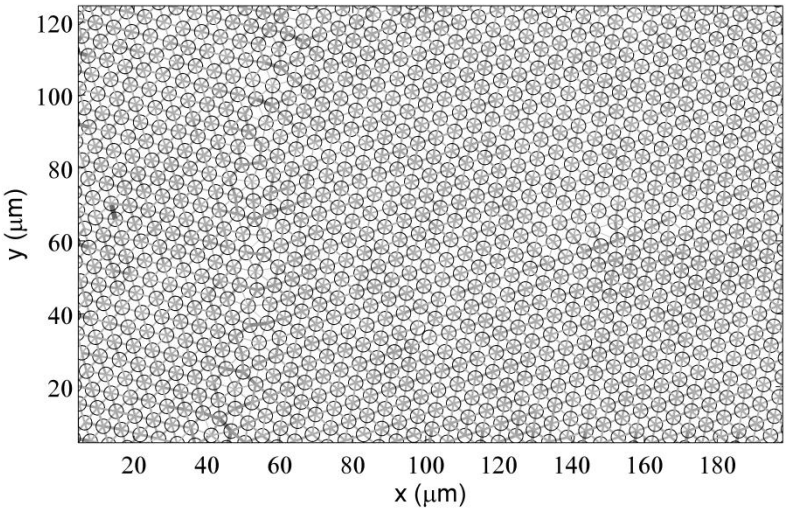

Figure 8|Force map constructed from a snapshot of the grain boundary in a crystal formed from silica particles. Larger forces are plotted with increasingly bold and dark lines.

3.5 SHEAR RELAXATION MODULUS

The level of homogeneity, as investigated in Section 3.1-3.4, in a material has a large influence on the dynamics and mechanical properties of a material. Key to understanding the dynamics of any material, is understanding the time dependent mechanical response. Thus far, measuring the mechanical properties of supersoft solids posed a challenge because the available methods are based on assumptions which don't hold in Wigner crystals. Here, we measure the shear relaxation of a 2D colloidal crystal, to our best knowledge for the first time, without assumptions or perturbations, and use our results to determine the phase of Wigner crystals.

In literature, the shear modulus of 3D colloidal dispersions is measured by perturbing the bulk[1], and a model is proposed to calculate the shear modulus.[19] We use a different method than previously reported, as described in Section 2.4. With the forces between every pair of particles known, we can compute and evaluate the visco-elastic properties of a sample without making any assumptions or actively perturbing the system. We propose a non-perturbative method to measure the elasticity in 2D colloidal systems, and use Equations 2-4 to calculate the shear modulus. We treat the fluctuations of the particles around their equilibrium positions as imposed shear, and assess the reaction of the system to this local deformation.

Materials with long-range ordering tend to relax slower after applying shear when compared to heterogeneous materials. When a deformation is applied, a material is not instantly in equilibrium, i.e. relaxed. Relaxation of the material can follow different trends, through which we can distinguish between phases. Solids don't relax after applying shear, whereas liquids have very fast exponential relaxation. Visco-elastic materials are subdivided in visco-elastic solid, which exhibits partial relaxation to a plateau, and visco-elastic liquid, which relaxes linearly.

Due to poor statistics at times relevant for relaxation, we are unfortunately unable to prove whether the system studied here is a visco-elastic liquid or solid, or make an estimate of the zero shear modulus in the case of a visco-elastic solid (Figure 9). We are, however, able to estimate the infinite shear modulus by extrapolation: 10-20mPa, which is within the expected range of μPa-mPa we hypothesised in the introduction. It is surprising that the infinite shear modulus for

the liquid and crystal are the same according to this measurement, and that the shear modulus for the liquid exceeds the modulus for the crystal between approximately 1 and 5 seconds.

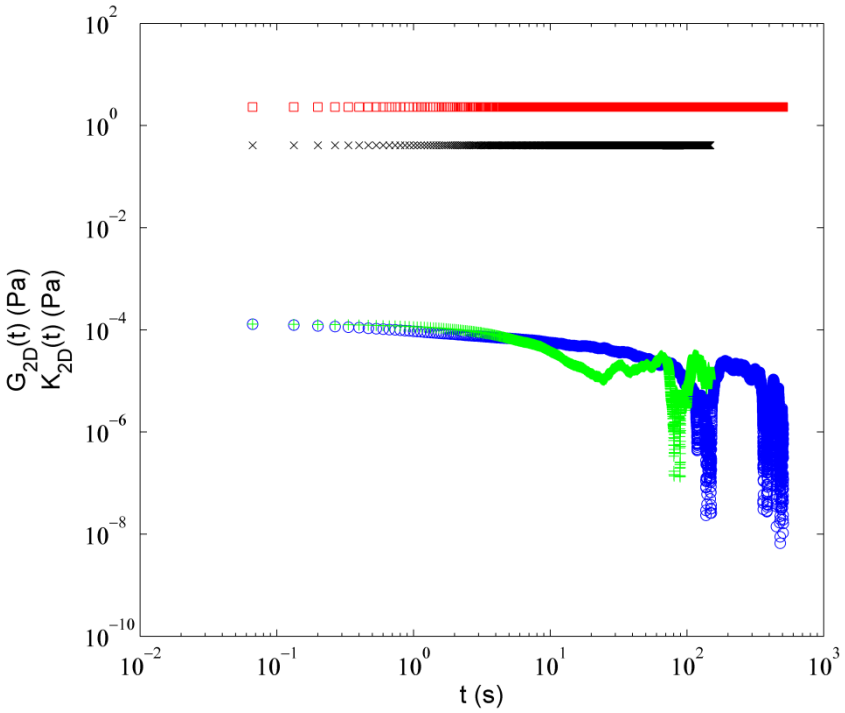

Figure 9|Relaxation of the shear modulus ($G_{2D}(t)$, blue circle), and compression ($K_{2D}(t)$, red square) in a crystal with a number density of $1.8 \cdot 10^{-2}$ particles per μm², and relaxation of the shear modulus ($G_{2D}(t)$, green plus), and compression ($K_{2D}(t)$, black cross) in a liquid with a number density of $4.4 \cdot 10^{-3}$ particles per μm².

For the liquid, when data-analysis is repeated with a larger data-set (data not shown), the shear modulus is approximately 3 decades higher than the modulus for the crystal, but the relaxation time does not change. This indicates that our algorithm is not error-free. For the liquid, we expect full relaxation of the shear if measurements are repeated. We hypothesise that the $G_{2D}(t)$ for a solid does not fully relax, but rather relaxes to a finite plateau, indicative for visco-elastic solids.

We also calculate the compression of the sample, using Equation 7. The compression does not change over time, and is several orders of magnitude higher than the modulus, which further enforces our claim of correctly measuring the shear modulus.

In the crystal we find a relaxation time of approximately 100 seconds(Figure 9). Because the particles in the liquid have a higher mobility compared to particles in the crystalline phase, we expect significantly faster relaxation in the liquid. In accordance with our expectations, we find a relaxation time of approximately 10 seconds.

3.6 Mean square displacements

Irrefutably determining the phase of Wigner crystals in Section 3.5 is hindered by poor statistics at time scales important for determining the relaxation time and the level of relaxation at long time scales, which we need to distinguish between visco-elastic solid and visco-elastic liquid. We supplement the information obtained by measuring the shear relaxation by calculating mean

square displacements of particles in both phases. The MSD in two dimensions is related to τ via Equation 10:

$$\langle r^2 \rangle = 4D\tau^{\alpha} \tag{10}$$

For a liquid we expect diffusive behaviour with α equal to 1, yielding a slope of 1 for the MSD plotted on log-log scale. For a solid we expect to find a plateau in the MSD, which indicates caging of particles by their neighbours. At short time scales, we expect to find subdiffusive behaviour for the solid, as the fluctuations around the equilibrium positions are slowed down, compared to diffusion, by repulsion by neighbouring particles.

In Figure 10 we plot the MSD for both the liquid and the crystalline samples. We find diffusive behaviour for the particles in the liquid phase. For the crystal we find subdiffusive behaviour at short times, and a plateau in the MSD for longer times, indicating that the crystalline phase of the supersoft solid studied here is indeed a solid. This gives further credibility to our hypothesis that Wigner crystals behave as visco-elastic solids under shear.

With establishing the solid phase of the Wigner crystals through analysis of the MSD, we can make a prediction of the evolution of the shear modulus of the crystal at longer time scales (Figure 10). We predict that, when measurements on this system are repeated and longer recordings are analysed, the system will relax to a finite plateau in the shear, as is characteristic of a visco-elastic solid.

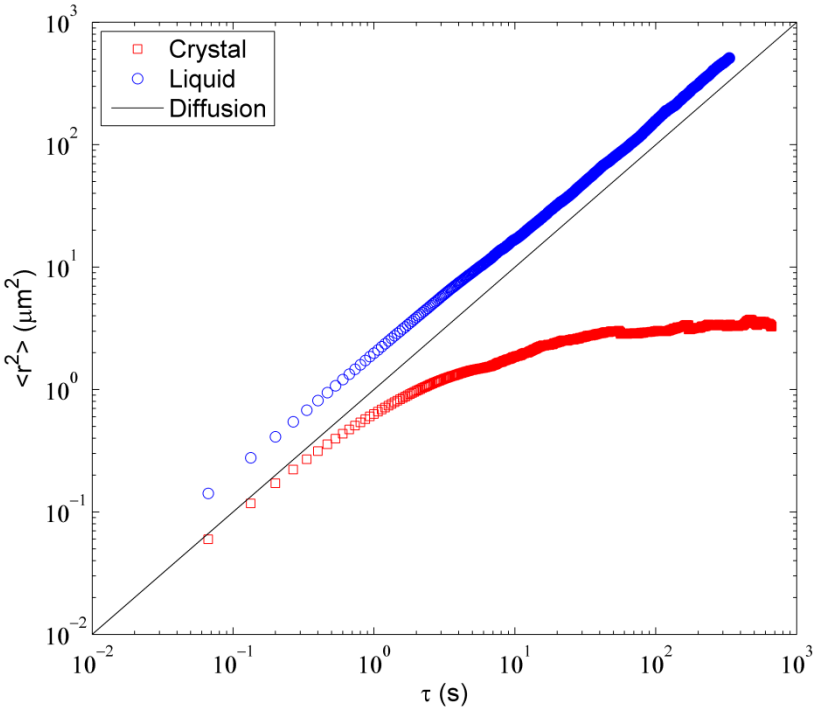

Figure 10|Mean square displacements for crystal (red squares) and liquid (blue circles). The black line indicates the slope for diffusive behaviour.

In this research we demonstrate and validate a novel approach to measure the mechanical properties of a supersoft solid. Using the parameters obtained from fitting our experimentally obtained pair potential to a Yukawa-type screened-Coulomb potential, we calculate interparticle

forces without making assumptions. We use the interparticle forces to calculate the 2D shear without interactions or perturbations for the first time, to the best of our knowledge. To support our hypothesis that Wigner crystals are supersoft solids, based on measurements of the shear relaxation, we assess the mean square displacements of the particles. From analysis of the MSDs, we conclude that Wigner crystals form visco-elastic solids, thus verifying our hypothesis.

4. CONCLUSIONS

In this research we pioneer a facile method to measure system parameters, such as shear modulus, without assumptions and perturbations. This method is based on our ability to directly measure the force between particle pairs as a function of their separation distance, by using a Yukawa-type screened Coulomb potential. The method described here requires considerably less experimental work than the other briefly discussed methods, extrapolation from dilution series and optical tweezer experiments. The only requirement for the method used in this thesis is sufficient dilution of the sample and sufficient data statistics. We like to point out that the exponential relation between interparticle force and centre-to-centre separation distance calls for very accurate particle locating.

In this research we expected to find force networks in the crystalline phase, to the example of the force networks found in granular materials by Snoeijer et al.[11] Snoeijer and co-workers, however, used hard spheres in their research, in which very small imperfections on the surfaces of the particles cause an imbalance in forces upon contact, yielding a force network. The particles used here, are not hard spheres, but have a shell surrounding each particle where other particles hardly venture because of the repulsion between the particles. The force between two particles brought closer together by thermal fluctuations is, of course, larger than the equilibrium force in the crystal, but not significant enough to form measurable force chains.

The high plasticity of the PMMA Wigner particles studied here may also prevent force networks from forming. The small difference in density between solvent and particle enables high mobility, in all three dimensions. These particles are mobile enough to redistribute relatively large forces, if the crystal is perturbed locally, by fast rearrangement of the surrounding particles, thus distributing forces over multiple bonds, or out-of-plane movement. The crystals studied here are not confined, but rather induced by gravitation acting on slightly tilted samples. Confinement of a denser crystal may yield force chains, as will be discussed in the next section.

We report preliminary results of non-perturbing measurements of the elastic properties of a 2D supersoft solid. Although we are not able to distinguish between visco-elastic liquid and visco-elastic solid from shear relaxation measurements as presented here, in combination with the MSD of the crystal we confirm our hypothesis: the crystalline phase is a visco-elastic solid. To our knowledge, this is the first time the shear relaxation is measured in 2D systems without active perturbation of or direct interaction with the material. We see a clear difference in relaxation times between the liquid and the solid, and validate our method by comparison with MSD analysis.

5. FUTURE RESEARCH

To properly determine which method is most suited for extracting the Yukawa parameters from experimental data, further experiments are needed. Image sequences should be recorded using brightfield, fluorescence and phase contrast microscopy, and the obtained parameters should be compared to each other and parameters obtained though optical tweezer experiments. These measurements should be performed on the same sample to eliminate effects of the density on the pair potential.

The force networks as described by Snoeijer et al. for granular matter[11] were realised in a hard sphere system, which is by definition different from Wigner crystals. Maybe if we use Wigner particles with a very steep pair potential, we could realise force networks. Another method would be to have the particles approach each other more closely, thus increasing the interparticle forces. To achieve this, we propose using particles with a larger difference in densities between solvent and particles so that the system is not as plastic and can become more dense than the PMMA crystals studied here. Another method to obtain force networks is mimicking granular matter by using a bidisperse mixture of colloidal Wigner particles. By experimenting with different ratios between the different sizes, and the volume ratio between the populations, it should be possible to obtain force networks in Wigner systems. A better understanding of these artificially obtained force networks may help in selecting criteria for formation of force networks in monodisperse Wigner crystals.

If we are able to realise force networks in Wigner systems, the next step would then be to study them in more detail. Force networks may, for example have strong directionality, indicating compression or shear in a specific directions. It would also be interesting to study the directionality of the force network surrounding large defects, such as grain boundaries. Studying the networks surrounding defects may provide useful information on the stability of the defects, and thus the 'healing' properties of the material. When actively manipulating the system, using for example optical tweezers, one could investigate the effects of compression, shear and confinement to finite sized crystals on the directionality and stability of the defects.

Preliminary results from this study indicate the existence of collective displacements of particles through thermal excitation in Wigner crystals, as reported in literature.[18] Further research may be conducted to analyse the stability, directionality, patterns, and (auto-)correlation in space and time of these collective movements.

This particular point may not be a matter of research, but more of the equipment used in these experiments. For the study of, especially, the shear relaxation and (auto-)correlation, image sequences covering more time are needed to obtain good statistics at time scales relevant for relaxation. In this project, we are limited by storage space. By using real-time particle tracking we would decimate the storage space needed for these data-sets, as the raw images wouldn't have to be saved. Using real-time tracking on the system used here poses more difficulties than just acquiring the proper instrumentation. The image sequences recorded in this research have been modified to enhance contrast and facilitate proper tracking. For real-time tracking, the raw image quality would have to be improved to allow proper detection of the particles.

The method described here to assess the shear relaxation of colloidal systems is by no means optimised. We pointed out that the comparison between shear moduli of a liquid and a crystal

indicates that our algorithm still contains errors. In order to study the shear relaxation of these systems in more detail, not only do we need to correct our algorithm and record longer data-sets, a higher frame rate so that we can sample the shear and MSD at shorter timescales would also benefit this particular part of the research. As the field of view would still need to be of sufficient size, combination with real-time tracking poses a challenge. In any case, a very fast computer is required to properly repeat these experiments.

Using optical tweezers, we can disrupt the ordering in the crystal at small and large scale. It would be interesting to investigate the shear relaxation of such a disrupted crystal.

It may be argued that the sample in the crystalline phase could still exhibit diffusive behaviour at longer time scales, but we do not expect this. By recording longer data-sets, we could establish the phase, visco-elastic solid, with more certainty, using both the MSD and shear relaxation analysis.

6. ACKNOWLEDGEMENTS

Ruben, I don't know what about you, but I genuinely enjoyed this thesis. Borrels and coffee breaks were sometimes inconveniently interrupted by doing research, but I couldn't have pulled this off without you. Thanks for supervising me. Thanks of always helping me when I needed you to, thanks for trying to teach me how to Matlab (and how to verbify), thanks for getting me through this thing, and thanks in general for the good time. Maybe I have to thank you most for putting up with me; I'm sorry for not sticking to the 5 o'clock rule.

Joris, thanks for supervising me during yet another thesis. I've worked under your supervision for about a year now, and you were always patient enough to elaborate when the name of the theory/formula/method didn't ring any bells, (which happened a lot) knowing exactly where I got lost and which details or analogues would make me understand. Thank you for guiding me through another six months of research and steadily teaching me to be more and more independent.

Jasper, thank you for your overall involvement in this project and for putting so much time in rewriting Matlab scripts. And thank you for providing me with such a nice and relaxed working environment for the past year.

Ties, somehow, 'houdoe en bedankt' doesn't quite cut it. Thanks for, usually, improving ~someone's~ mood when you're around. Thanks for the good times, the pepernoten-dinner, the hot chocolate and for time-sharing Ruben.

Suus and Max, although you've both been abroad during most of my thesis, you really supported and encouraged me, and were able to talk me through another thesis. Just before I started on this project, you both flew back to The Netherlands to join me at Pinkpop, which was again factor 5 awesome. That weekend really got me relaxed and recharged enough to start another thesis. I propose we make Pinkpop a tradition, I think we could all use a festival by that time next year.

Jeroen and Jan Bart, you guys may not have been my supervisors, or helped me with the research part of my thesis, but you did your part in making the past six months more fun. Thanks, Jan Bart, for doing some of the most important groceries of the week. And if it wasn't for you, Jeroen, I don't think I would have barbequed much this year, so, thanks.

Thanks to FYSKO and BioNT for the great time I've had here. After such a long time it will be weird not to come to the lab every day.

7. REFERENCES

[1] H. M. Lindsay, P. M. Chaikin, The Journal of Chemical Physics 1982, 76, 3774.

[2] E. M. Furst, Soft Materials 2003, 1, 167.

[3] M. J. Solomon, Q. Lu, Current Opinion in Colloid & Interface Science 2001, 6, 430.

[4] L. G. Wilson, A. W. Harrison, A. B. Schofield, J. Arlt, W. C. K. Poon, Journal of Physical Chemistry B 2009, 113, 3806.

[5] A. S. Dukhin, P. J. Goetz, Advances in Colloid and Interface Science 2001, 92, 73.

[6] A. E. Larsen, D. G. Grier, Nature 1997, 385, 230.

[7] F. M. Peeters, X. G. Wu, Physical Review A 1987, 35, 3109.

[8] R. Rajagopalan, K. S. Rao, Physical Review E 1997, 55, 4423.

[9] J. C. Crocker, D. G. Grier, Physical Review Letters 1994, 73, 352.

[10] C. R. Iacovella, R. E. Rogers, S. C. Glotzer, M. J. Solomon, Journal of Chemical Physics 2010, 133.

[11] J. H. Snoeijer, T. J. H. Vlugt, M. van Hecke, W. van Saarloos, Physical Review Letters 2004, 92.

[12] L. Antl, J. W. Goodwin, R. D. Hill, R. H. Ottewill, S. M. Owens, S. Papworth, J. A. Waters, Colloids and Surfaces 1986, 17, 67.

[13] M. Kilfoil, 2014.

[14] M. Guizar-Sicairos, J. C. Gutierrez-Vega, Journal of the Optical Society of America a-Optics Image Science and Vision 2004, 21, 53.

[15] R. Higler, J. Appel, J. Sprakel, Soft Matter 2013, 9, 5372.

[16] W. R. Bowen, A. O. Sharif, Nature 1998, 393, 663.

[17] J. Baumgartl, J. L. Arauz-Lara, C. Bechinger, Soft Matter 2006, 2, 631; J. Baumgartl, C. Bechinger, Europhysics Letters 2005, 71, 487.

[18] B. van der Meer, W. Qi, R. G. Fokkink, J. van der Gucht, M. Dijkstra, J. Sprakel, Proceedings of the National Academy of Sciences 2014.

[19] K. Ito, K. Sumaru, N. Ise, Physical Review B 1992, 46, 3105.

[20] H. Yang, P. Pi, Z.-Q. Cai, X. Wen, X. Wang, J. Cheng, Z.-r. Yang, Applied Surface Science 2010, 256, 4095.

APPENDIX

A1 SiO_2 PARTICLES

PARTICLE MODIFICATION

This protocol is modified from an existing protocol.[20] Suspend ~1g 4µm SiO2 particles in a mixture of EtOH/NH_4OH/H_2O with molar ratio 7/0.5/5.3 by sonication for 1hr. Add 0.35ml (1.6mmol) TEOS and 1.34ml (6.39mmol) HMDS and sonicate for 10min, then stir the reaction mixture for 16hrs at 60°C. Sonicate the mixture for 10 min, and allow reaction to continue for 3hrs. Stop the reaction by cooling to rt and sedimenting the particles. Wash the particles twice in the EtOH/NH_4OH/H_2O mixture, then dry them in a 65°C stove for 22hrs, and then in a 50°C vacuum oven for 1.5hrs. Resuspend the particles in 10mM AoT in tetralin by sonicating for 30 min and repeat the sedimentation step until the suspension is clean.

PAIR POTENTIAL SiO_2 PARTICLES

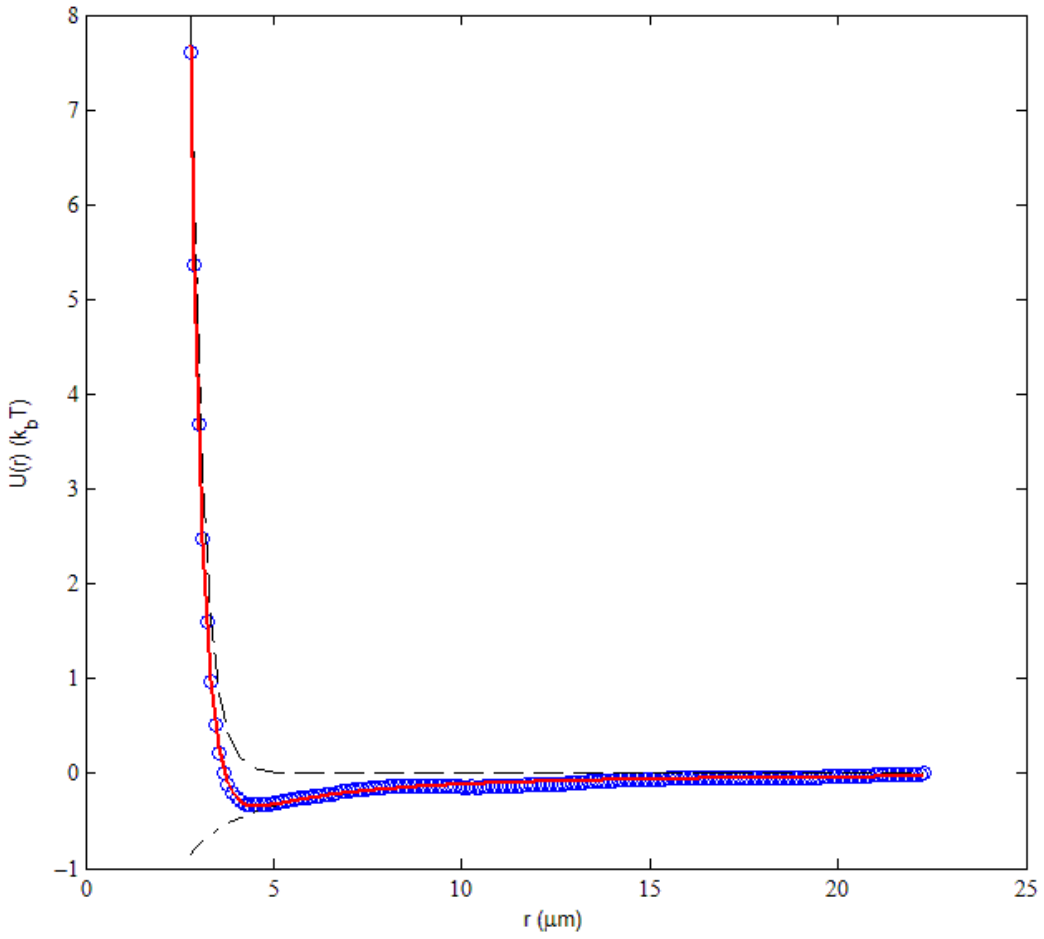

Figure A1|Yukawa potential for SiO_2 particles in 10mM AoT in tetralin. The blue circles are obtained experimental data, the red line is the fit with the modified Yukawa potential composed of the modelled Yukawa potential with obtained fitting parameters (black dashed line) and a powerlaw (black dash dot).

A2 PAIR POTENTIAL PMMA PHASE CONTRAST

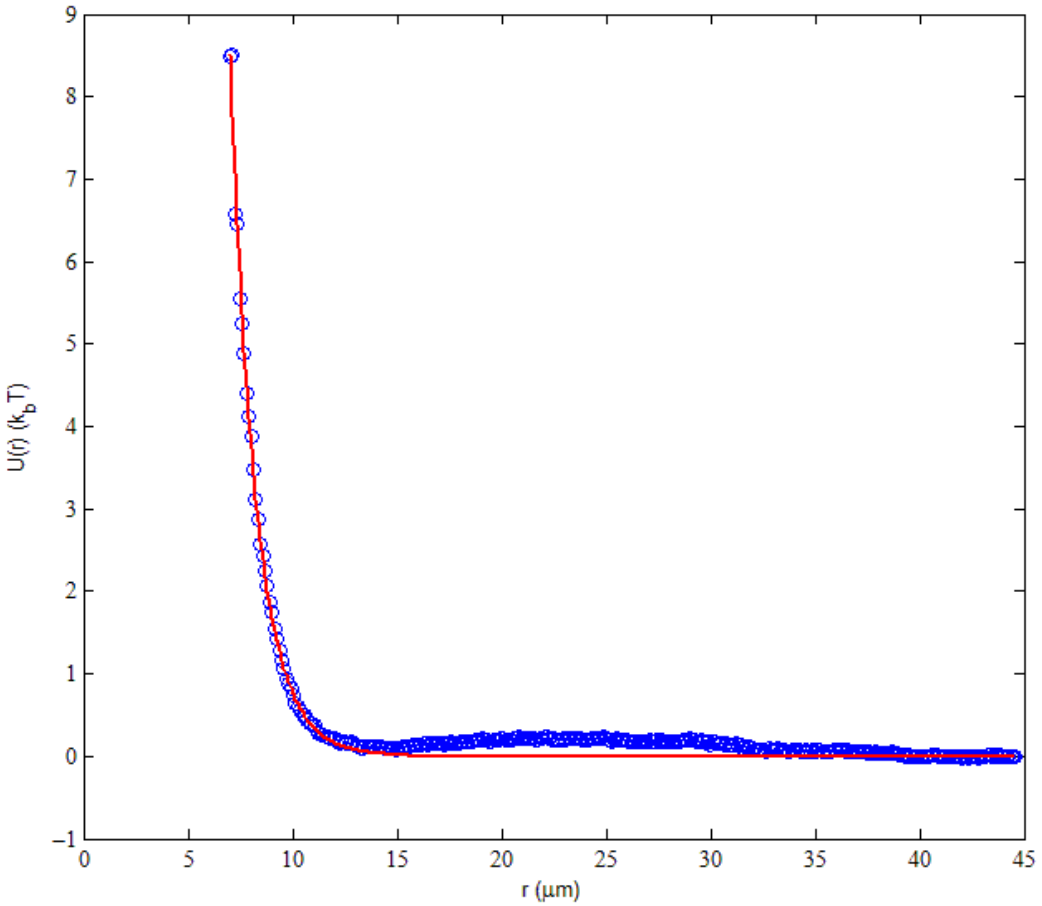

Figure A2|Pair potential obtained from a dataset recorded in brightfield mode with phase contrast filter (blue circles) and the modelled Yukawa potential with obtained fitting paramters (red line). Data-set is recorded at 15 fps. The number density of this sample is $2.0 \cdot 10^{-3}$ particles per μm^2.

A3 FORCE DISTRIBUTION IN SiO_2 CRYSTAL

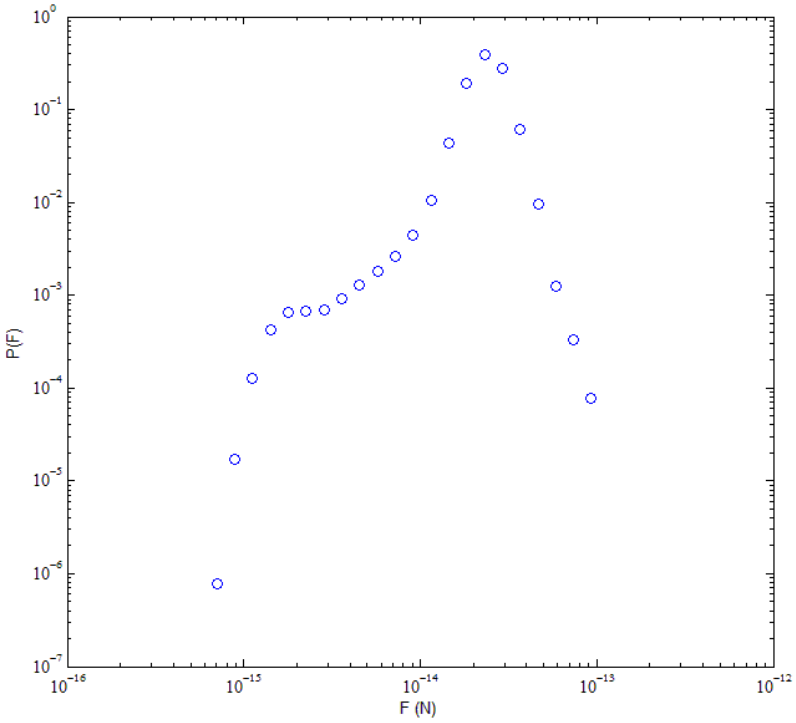

Figure A3|Force distribution of a crystal of silica particles, containing a grain boundary. The number density in this crystal is $4.0 \cdot 10^{-2}$ particles per μm^{-2}.